JOURNAL OF CATALYSIS 95, 181–192 (1985)

Supported Liquid-Phase Catalysis

I. A Theoretical Model for Transport and Reaction

RAVINDRA DATTA* AND ROBERT G. RINKER†

Chemical and Materials Engineering Department, University of Iowa, Iowa City, Iowa 52242, and †Department of Chemical and Nuclear Engineering, University of California, Santa Barbara, California 93106

Received October 16, 1984; revised April 11, 1985

A simplified theoretical model is proposed for the transport and chemical reaction of gaseous species in supported liquid-phase catalysts (SLPC) in which catalytic liquids with contact angles less than 90° are dispersed within inert porous supports. It is based on the use of the dusty-gas model for the flux in the residual gas pore space. The variation of the structural dusty-gas parameters with liquid loading is correlated by using results borrowed from the parallel-pore model and the random-pore model along with an interconnected near-spherical cell description of the porous medium. The proposed model is free of adjustable parameters and is therefore predictive. It corroborates the existence of a maximum in the reaction rate predicted previously for some systems and also exhibits other trends observed experimentally. In addition, other interesting characteristics of SLPC are predicted.

I. INTRODUCTION

Supported liquid-phase catalysis (SLPC) consists of a liquid-phase catalyst dispersed within a porous support so as to occupy a part of the pore space. The gaseous reactants diffuse through the residual pore space as well as the dispersed liquid phase and undergo homogeneous catalytic reaction in the liquid phase to produce volatile products, which then diffuse back out of the porous support.

It is thus a hybrid system that retains the advantages of homogeneous catalysts such as higher stability, product selectivity, and milder operating conditions and, at the same time, provides the advantages of heterogeneous catalysts such as convenient handling, large interfacial areas, and consequently small liquid diffusion paths, ease of separation of catalyst and product, and use of conventional equipment like packed-bed and fluidized-bed reactors. Its major limitation is that the reactants and the products must be in gaseous or vapor form at reaction conditions while the catalyst solution should be essentially nonvolatile.

There are a growing number of examples of the application of the SLPC technique (*1–6*). These include (a) oxidation of SO_2 by supported melts of alkali-promoted V_2O_5 in the manufacture of sulfuric acid; (b) polymerization and alkylation by phosphoric acid impregnated on Kieselguhr; (c) oxidation of HCl to Cl_2 and oxychlorination of olefins by the Deacon catalyst, which is a melt of $CuCl_2$/CuCl/KCl/rare-earth halides supported on pumice or silica gel; and (d) oxidation of ethylene to acetaldehyde catalyzed by a supported aqueous solution of $PdCl_2$ and $CuCl_2$. In addition, the technique has considerable potential for industrial application in the rapidly growing field of homogeneous catalysis by transition-metal complexes for a wide variety of hydrocarbon conversions (*7*). It has successfully been demonstrated in the laboratory for reactions such as hydroformylation (*8, 9*), isomerization (*10, 11*), and hydrogenation (*11*).

0021-9517/85 $3.00

The first theoretical model for diffusion and reaction in SLPC (*12*) was based on a cylindrical pore containing the catalytic liquid as a film at the mouth and as a plug at the other end of the pore. An arbitrary liquid distribution function containing two adjustable parameters was chosen which satisfied the limiting characteristics of the actual distribution. The model showed that there should be optimum liquid loading and a corresponding maximum in the reaction rate for SLPC which was later qualitatively confirmed by experiments on propylene hydroformylation (*8*). However, while this first model includes many of the essential features of SLPC, it is not predictive because it involves adjustable parameters which have no physical basis.

Other SLPC models have been subsequently proposed (*3, 13, 14*), one of which (*3*) is also based on some arbitrary assumptions. Another of these models (*13*) is predictive and includes an empirical correlation for effective diffusivity as a function of liquid loading, based on isobaric diffusion experiments in liquid-impregnated pellets. The effective binary molecular diffusivity in the gas phase was found to be proportional to the square of residual porosity, but the treatment is limited to transport in the gas phase by ordinary molecular diffusion only.

The latest model (*14*), based on the dusty-gas concept (*15*), includes a realistic picture of liquid distribution based on the actual pore-size distribution of the dry support. Experiments indicated that the average liquid-film thickness in macropores is equal to the radius of the largest filled micropore. A further significant conclusion, based on experiments with three different liquids, was that the dispersion pattern of liquids having a contact angle less than 90° is essentially the same in an α-alumina support. The use of this model for predictive purposes, however, requires a knowledge of the pore-size distribution of the dry support from which the liquid distribution is then estimated.

It was our objective here to develop a relatively simple yet adequate theoretical model for the transport and reaction of gaseous species in SLPC that avoids use of adjustable parameters and involves tested assumptions. The proposed transport model requires a knowledge of the dusty-gas structural parameters for the dry porous support but is otherwise predictive.

2. PROPOSED MODEL

The activity of SLPC pellets depends on not only the amount of liquid present in the pellet but also the manner in which it disperses within the pores of the support. Some of the other factors that affect its activity are (a) pore-size distribution of the support, (b) the wetting characteristics of the liquid, (c) liquid-phase kinetics, (d) solubility of gaseous reactants and products in the liquid, (e) any catalyst–support interactions, and (f) perhaps even the method of preparation of SLPC.

Clearly, it is a formidable task to take all these factors into account. We, therefore, make some simplifying assumptions. It is assumed that (a) the porous support is completely inert; (b) the catalytic liquid wets the support, i.e., it has a contact angle $<90°$, (c) the liquid loading is uniform throughout the pellet, and (d) there is no surface diffusion. Additional assumptions concerning the liquid distribution and its effect on transport are given below.

While a quantitative description of the liquid distribution is not yet possible, the following picture emerges for wetting liquids based on thermodynamic considerations and experimental evidence (*1, 14*). At very low liquid loadings, the liquid is finely and evenly distributed as a thin film on the solid surface and is held by adsorption forces. As the loading increases further, the liquid gradually starts filling the capillary pores in order of the size distribution, filling the smallest pores first. Simultaneously, the thickness of the liquid film in the unfilled pores also increases but per-

haps reaches a limiting value due to the limited adsorption forces. As more liquid is introduced, the larger pores also gradually become filled with capillary liquid. We assume that the gas and the liquid phases are continuous and are in equilibrium at all points.

Introduction of a liquid into a porous solid reduces the residual gas-phase volume. Hence, it reduces the effective area for gas-phase transport and, further, increases the tortuosity factor for the residual gas phase by blocking off some of the pore interconnections. This effectively changes the porous structure for gas-phase transport. Thus, so far as the gas-phase transport is concerned, we can treat the support along with its dispersed liquid as a hypothetical porous medium with a new pore structure as determined by the liquid distribution. Similarly, when considering the transport in the liquid phase, we treat the gas phase together with the porous solid as the new hypothetical porous medium.

To use the existing theoretical flux models for describing transport in either the gas or the liquid phase in this hypothetical media, we need to know the effective porosity and tortuosity factors for the two phases. The effective porosity of a phase is, of course, readily obtained from the liquid loading, q, and the porosity of the dry support; but the tortuosity factor for the phase would depend upon the liquid distribution pattern as well as the pore structure of the support. For simplicity, we assume that the changes in tortuosity factors due to liquid loading for either of the phases can be estimated using the random-pore model (*16*) which, for monodisperse porous structures, gives the tortuosity as simply the inverse of porosity. In general a better estimate may be made by assuming $\tau = 1/\theta^{\alpha}$, where α varies between 1 and 2 depending upon the porous medium (*17*).

It is further assumed that the transport of a gaseous species, i, takes place in parallel in the two phases, so that the total flux of i in the pellet, N_i, is a sum of the individual contributions of the gas-phase flux, N_i^G, and the liquid-phase flux, N_i^L,

$$N_i = N_i^G + N_i^L. \tag{1}$$

(a) Flux in the Gas Phase

We assume that the transport of species i in the residual gas pore space is given by the dusty-gas model (*15*) having the form (*18*)

$$\frac{N_i^G}{D_{kie}^G} + \sum_{\substack{j=1 \\ j\neq i}}^{n} \frac{x_j N_i^G - x_i N_j^G}{D_{ije}^G} = -\frac{P}{R_g T}\frac{dx_i}{dz} - \frac{x_i}{R_g T}\left(1 + \frac{C_0^G P}{\mu_m D_{kie}^G}\right)\frac{dP}{dz} \qquad (i = 1, 2, \ldots, n), \tag{2}$$

where the superscript G refers to the residual gas pore space. The effective Knudsen diffusivity for the residual gas pore space is

$$D_{kie}^G = C_1^G v_i = C_1^G \left(\frac{8R_g T}{\pi M_i}\right)^{1/2}. \tag{3}$$

The effective binary pair molecular diffusivity is

$$D_{ije}^G = C_2^G D_{ij}. \tag{4}$$

It is convenient, for our purposes, to recast Eq. (2) into the Fickian form with an effective diffusivity for the residual gas pore space D_{ie}^G defined by

$$N_i^G = -\frac{P}{R_g T} D_{ie}^G \frac{dx_i}{dz} \qquad (i = 1, 2, \ldots, n). \tag{5}$$

To obtain an expression for D_{ie}^G some manipulations are required. Summing Eq. (2) for all n components causes the second term on the left-hand side to disappear. Multiplying and dividing by N_i^G we then obtain

$$N_i^G \sum_{j=1}^{n} \frac{N_j^G}{N_i^G}\frac{1}{D_{kje}^G} = -\frac{1}{R_g T}\left(1 + \frac{C_0^G P}{\mu_m D_{kme}^G}\right)\frac{dP}{dz} \qquad (i = 1, 2, \ldots, n). \tag{6}$$

where the mean effective Knudsen diffusion coefficient for the gas space is defined by

$$\frac{1}{D^{G}_{kme}} = \sum_{j=1}^{n} \frac{x_j}{D^{G}_{kje}}. \tag{7}$$

Using Eq. (6) in Eq. (2) to eliminate dP/dz and comparing the resulting expression to Eq. (5) results in

$$\frac{1}{D^{G}_{ie}} = \frac{1}{D^{G}_{kie}} + \sum_{\substack{j=1 \\ j\neq i}}^{n} \frac{1}{D^{G}_{ije}} \left(x_j - x_i \frac{N^{G}_{j}}{N^{G}_{i}}\right) - x_i \left\{\frac{1 + \dfrac{C^{G}_{0} P}{\mu_m D^{G}_{kie}}}{1 + \dfrac{C^{G}_{0} P}{\mu_m D^{G}_{kme}}}\right\} \sum_{j=1}^{n} \frac{N^{G}_{j}}{N^{G}_{i}} \frac{1}{D^{G}_{kje}} \quad (i = 1, 2, \ldots, n). \tag{8}$$

These equations are subject to the constraint that

$$\sum_{j=1}^{n} x_j = 1. \tag{9}$$

Thus, if the flux ratios in the gas phase N^{G}_{j}/N^{G}_{i} are known a priori as from reaction stoichiometry, for example, then the effective diffusivity D^{G}_{ie} remains a function of only the gas-phase mole fractions and pressure in addition to other constant parameters. Furthermore, simpler forms of D^{G}_{ie} can be obtained for many special cases. A rather important special case may be mentioned here. When the gaseous species involved are not of widely different molecular weights, the term contained within the braces in Eq. (8) is of the order of unity. Equating it to unity, Eq. (8) reduces to

$$\frac{1}{D^{G}_{ie}} = \frac{1}{D^{G}_{kie}} + \sum_{\substack{j=1 \\ j\neq i}}^{n} \frac{1}{D^{G}_{ije}} \left(x_j - x_i \frac{N^{G}_{j}}{N^{G}_{i}}\right) - x_i \sum_{j=1}^{n} \frac{N^{G}_{j}}{N^{G}_{i}} \frac{1}{D^{G}_{kje}} \quad (i = 1, 2, \ldots, n). \tag{10}$$

The advantage of Eq. (10) is that it does not contain the D'Arcy permeability C^{G}_{0} and, hence, involves one less structural parameter. In general, however, Eq. (5) along with Eq. (8) describes the flux of i in the gas phase of a partially liquid-impregnated porous pellet. The pressure inside the pellet is estimated by Eq. (6).

(b) *Variation of Structural Parameters with Liquid Loading*

In the above equations, the three dusty-gas constants, namely, C^{G}_{0}, the D'Arcy permeability, C^{G}_{1}, the Knudsen diffusion structural constant, and C^{G}_{2}, the molecular diffusion structural constant, all refer to the residual gas-pore space and, therefore, must vary with the extent and manner of liquid loading. If we compare the equivalent flux relationships given by the parallel-pore model, we may write (*18*)

$$C^{G}_{0} = \frac{\theta^{G}}{\tau^{G}} \frac{(a^{G})^2}{8} \tag{11}$$

$$C^{G}_{1} = \frac{2a^{G}}{3} \frac{\theta^{G}}{\tau^{G}} \tag{12}$$

and

$$C^{G}_{2} = \frac{\theta^{G}}{\tau^{G}}, \tag{13}$$

where θ^{G} is the porosity and τ^{G} is the tortuosity factor of the residual gas pore space for which the average pore size becomes

$$a^{G} = \frac{2\theta^{G}}{S^{G}\rho_p}. \tag{14}$$

These equations have been written for the residual gas pore space in a partially liquid-impregnated porous medium. If we write an analogous set of equations for the dry medium, designated by the superscript O, the following ratios result

$$\frac{C^{G}_{0}}{C^{O}_{0}} = \left(\frac{\theta^{G}}{\theta^{O}}\right)^3 \left(\frac{\tau^{O}}{\tau^{G}}\right) \left(\frac{S^{O}}{S^{G}}\right)^2 \tag{15}$$

$$\frac{C^{G}_{1}}{C^{O}_{1}} = \left(\frac{\theta^{G}}{\theta^{O}}\right)^2 \left(\frac{\tau^{O}}{\tau^{G}}\right) \left(\frac{S^{O}}{S^{G}}\right) \tag{16}$$

$$\frac{C^{G}_{2}}{C^{O}_{2}} = \left(\frac{\theta^{G}}{\theta^{O}}\right) \left(\frac{\tau^{O}}{\tau^{G}}\right). \tag{17}$$

Making use of the random-pore model (*16*), we obtain

$$\frac{\tau^G}{\tau^O} = \frac{\theta^O}{\theta^G}. \tag{18}$$

Next we try to find a relation between the gas–liquid interfacial area S^G and the residual porosity, θ^G. At this stage, however, it becomes necessary to be more specific about the physical model assumed for the porous structure and the liquid distribution. The simplest case would be to assume that the liquid forms uniform thin films on the walls of cylindrical pores without blocking off any of the pore interconnections. Then

$$\frac{S^G}{S^O} = \left(\frac{\theta^G}{\theta^O}\right)^{1/2}. \tag{19}$$

If, on the other hand, we visualize the pore structure as consisting of interconnected near-spherical "cells" (*19*) rather than tubular capillaries but still assume that the liquid forms a film on the internal surface, we obtain

$$\frac{S^G}{S^O} = \left(\frac{\theta^G}{\theta^O}\right)^{2/3}. \tag{20}$$

Although both Eqs. (19) and (20) are based on idealized models, we prefer to use the latter as it may be physically more realistic.

Finally, in terms of the liquid loading parameter, q,

$$\theta^G = \theta^O(1 - q). \tag{21}$$

Substituting Eqs. (18), (20), and (21) into Eqs. (15)–(17),

$$\frac{C_0^G}{C_0^O} = (1 - q)^{8/3} \tag{22}$$

$$\frac{C_1^G}{C_1^O} = (1 - q)^{7/3} \tag{23}$$

$$\frac{C_2^G}{C_2^O} = (1 - q)^2. \tag{24}$$

Experimental confirmation of these equations is considered in Part II.

(c) *Flux in the Liquid Phase*

The effective diffusion coefficient in a completely liquid-filled pellet is usually given by (*20*)

$$D_{ie} = \frac{\theta}{\tau} D_i^L = C_2^O D_i^L. \tag{25}$$

In an analogous fashion we may write the flux in the liquid phase of a partially liquid-filled pellet as

$$N_i^L = -D_{ie}^L \frac{dC_i^G}{dz} = -\frac{P}{R_gT} D_{ie}^L \frac{dx_i}{dz} - \frac{x_i}{R_gT} D_{ie}^L \frac{dP}{dz} \qquad (i = 1, 2, \ldots, n) \tag{26}$$

where the effective diffusivity in the liquid phase becomes

$$D_{ie}^L = \frac{\theta^L}{\tau^L} D_i^L H_i = C_2^L D_i^L H_i. \tag{27}$$

The partition coefficient H_i has to be included here since Eq. (26) has been written based on the gas-phase concentration gradient. Also, θ^L and τ^L now correspond only to the liquid phase in the pores. If we assume a relation similar to Eq. (18) for the liquid-phase tortuosity, then

$$\frac{C_2^L}{C_2^O} = q^2. \tag{28}$$

(d) *Transport and Reaction in SLPC*

We consider a mixture of n gaseous species, the first m of which participate in a single homogeneous liquid-phase isothermal catalytic reaction in SLPC:

$$\sum_{i=1}^{m} \nu_i A_i = 0. \tag{29}$$

The rest of the species are assumed to be inert. The steady-state differential material balance in SLPC takes the form

$$\frac{1}{z^h} \frac{d}{dz}(z^h N_i) = \theta q \nu_i R \qquad (i = 1, \ldots, m), \tag{30}$$

where it has been assumed that the average liquid-film thickness is small enough so that the effectiveness factor for the liquid film is essentially unity. The shape factor $h = 0$, 1, and 2 for the planar, cylindrical, and spherical geometries of the pellet, respectively.

For the inert species

$$\frac{1}{z^h}\frac{d}{dz}(z^h N_i) = 0 \qquad (i = m+1, \ldots, n). \quad (31)$$

These equations are subject to the boundary conditions

$$z = 0; \qquad N_i = 0 \quad (32)$$

$$z = L; \qquad x_i = x_{is}, P = P_s. \quad (33)$$

In general, under isothermal conditions, the rate of chemical reaction per unit volume of the liquid phase, R, is a function only of the concentrations of the reacting species in the liquid phase. This can be related to the local gas-phase composition assuming equilibrium. Thus

$$R = R(x_i, P) \qquad (i = 1, 2, \ldots, m). \quad (34)$$

For inert components, Eq. (31) yields

$$N_i = 0 \qquad (i = m+1, \ldots, n). \quad (35)$$

For the reacting species, the fluxes are related by stoichiometry

$$N_i/N_j = \nu_i/\nu_j \qquad (i = 1, \ldots, m). \quad (36)$$

Thus, Eqs. (30), (35), and (36) along with the flux model Eqs. (1), (5), (6), (8), (26), and (27) represent the complete model for transport and single reaction of gaseous species in SLPC. Their solution leads to the effectiveness factor defined by

$$E_p = \frac{(h+1)N_{is}}{L\nu_i R(x_{is}, P_s)}. \quad (37)$$

This completes the general formulation of the problem.

3. ILLUSTRATIVE EXAMPLE

We consider next a simple example of diffusion and reaction in SLPC to highlight the salient features of the above theoretical model. The example considered involves a single, irreversible, first-order, homogeneous, catalytic reaction in the liquid phase of gaseous reactant A to form the gaseous product B in the presence of a large excess of an inert gas I, e.g., an isomerization reaction,

$$A \rightarrow B.$$

Such a test reaction for SLPC has been suggested (*21*).

For this case, Eq. (8), along with Eq. (36) (and assuming $N_i/N_j = N_i^G/N_j^G$), yields

$$\frac{1}{D_{Ae}^G} = x_I\left(\frac{1}{D_{AIc}^G} - \frac{1}{D_{ABc}^G}\right) + \frac{1}{D_{ABe}^G} + \frac{1}{D_{kAe}^G}. \quad (38)$$

Further, since $M_A = M_B$, $dP/dz = 0$, from Eq. (6); i.e., the pellet is isobaric. Thus, substituting Eqs. (5) and (26) into Eq. (1), we may write the overall flux as

$$N_A = -D_{Ae}\frac{dC_A^G}{dz} \quad (39)$$

where $D_{Ae} = D_{Ae}^G + D_{Ae}^L$. Substituting the appropriate equations, in terms of liquid loading, finally,

$$D_{Ae} = \frac{C_2^O(1-q)^2}{x_I\left(\frac{1}{D_{AI}} - \frac{1}{D_{AB}}\right) + \frac{1}{D_{AB}} + \frac{1}{(1-q)^{1/3}D_{kA}} + C_2^O H_A D_A^L q^2}, \quad (40)$$

where

$$D_{kA} = \frac{C_1^O}{C_2^O}\left(\frac{8R_gT}{\pi M_A}\right)^{1/2}. \quad (41)$$

Further, since $x_I \rightarrow 1$, we may assume it to be constant. Then Eq. (30) may be solved directly for a first-order irreversible reaction (*22*):

$$E_p = \left(\frac{h+1}{\phi_p}\right)\frac{I_{\frac{h+1}{2}}(\phi_p)}{I_{\frac{h-1}{2}}(\phi_p)} \quad (42)$$

where the Thiele modulus ϕ_p is

$$\phi_p = L\left(\frac{q\theta^O H_A k_A}{D_{Ae}}\right)^{1/2}. \quad (43)$$

Equation (42) reduces to the appropriate expressions for planar, cylindrical, and spherical geometries for the shape factor $h = 0$, 1, and 2, respectively.

Equation (43) is rearranged and written as

$$\phi_p = \phi_p^L \left(\frac{qC_2^O H_A D_A^L}{D_{Ae}}\right)^{1/2}, \qquad (44)$$

where the Thiele modulus for the completely liquid-filled pellet ($q = 1$) is

$$\phi_p^L = L\left(\frac{\theta^O k_A}{C_2^O D_A^L}\right)^{1/2}. \qquad (45)$$

The rate of reaction per unit external surface area for the SLPC pellet becomes

$$r_A = \left(\frac{L}{h+1}\right)\theta^O q H_A k_A C_{As}^G E_p. \qquad (46)$$

Finally, it is convenient to write the rate of reaction, r_A, as a ratio involving the rate for a completely liquid-filled pellet, r_A^L. Thus,

$$r_A' = \frac{r_A}{r_A^L} = q\frac{E_p}{E_p^L} \qquad (47)$$

where E_p^L is the effectiveness factor for a completely liquid-filled pellet.

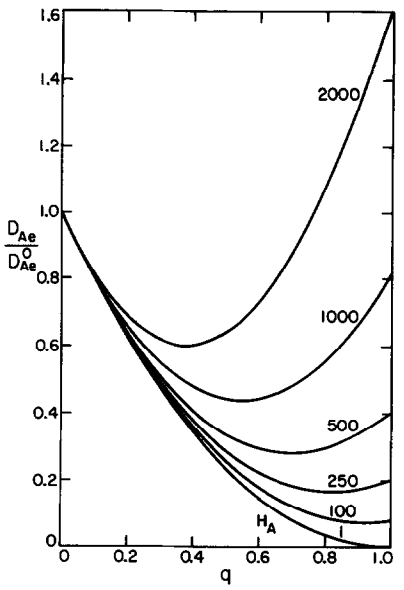

FIG. 1. The ratio of the effective diffusivity in a liquid-loaded pellet to the effective diffusivity in the dry pellet, versus the liquid loading.

4. RESULTS AND DISCUSSION

The expressions obtained for the example illustrated above are next used to study the behavior of SLPC systems. The effect of liquid loading q on the flux of a gaseous species in liquid-impregnated porous media can be illustrated by plotting the overall effective diffusivity, D_{Ae}, given by Eq. (40), as a ratio relative to the effective diffusivity, D_{Ae}^O, for the dry support, obtained by substituting $q = 0$ in Eq. (40). This ratio is plotted in Fig. 1 versus the liquid loading, using values for the gas and liquid diffusivities such as 2.7×10^{-6} m^2/s for D_{AB}, 8.8×10^{-6} m^2/s for D_{AI}, 2.5×10^{-5} m^2/s for D_{kA}, and 4.4×10^{-9} m^2/s for D_A^L. For gases of low solubility in the liquid, the partition coefficient is small, e.g., $H_A = 1$ or less, and the liquid-phase contribution to the overall transport is negligible. The curve for $H_A = 1$, therefore, essentially coincides with the curve $(1 - q)^2$. For a gas having a higher partition coefficient, the flux contribution of the liquid phase becomes significant and the diffusion in a completely filled pellet may no longer be negligibly small. As H_A increases further, the diffusivity curves shift upward and also describe a minimum in the effective diffusivity which shifts toward lower liquid loadings with increasing H_A. Finally, the effective diffusivity may even exceed that for the dry pellet as the solubility increases further, e.g., see the curve for $H_A = 2000$. It may be noted that the range of H_A from unity to 2000 used in Fig. 1 is not unrealistic. Many hydrocarbon vapors and gases have partition coefficients between 50 and 500. Vapors of substances that exist as liquid around room temperatures have H_A of 2000 or more.

For most gaseous solutes, the ratio of the liquid-phase diffusivity to the gas-phase diffusivity remains of the order of $\sim 10^{-4}$, whereas the other parameters, H_A and k_A, may vary over a wide range. For this reason, we assume a set of values of the diffusivities that we believe are typical, and maintaining these constant, we vary H_A and ϕ_p^L (or k_A) over a wide range in order to fully

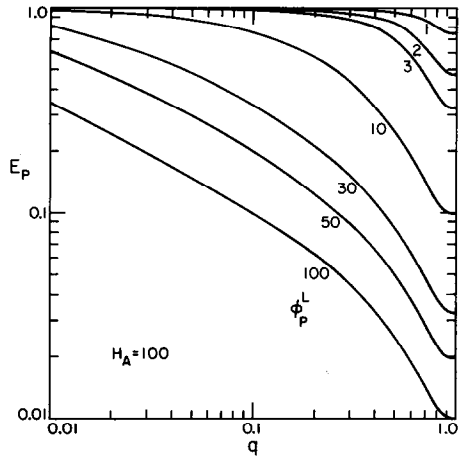

FIG. 2. The effectiveness factor for SLPC slab versus the liquid loading for $H_A = 100$ and ϕ_p^L varying from 1 to 100.

elucidate the possible behavior of SLPC systems.

Figure 2 shows the effectiveness factor for SLPC for slab geometry versus the liquid loading for a constant value of $H_A = 100$ and ϕ_p^L varying from 1 to 100. In Fig. 3, ϕ_p^L is maintained constant at 20 while H_A varies from 1 to 2000. E_p reduces with increasing H_A, the curves passing through a minimum before reaching the value $E_p = 1/\phi_p^L$ for $q = 1$. This behavior is merely a reflection of the variation of D_{Ae} with q for large H_A.

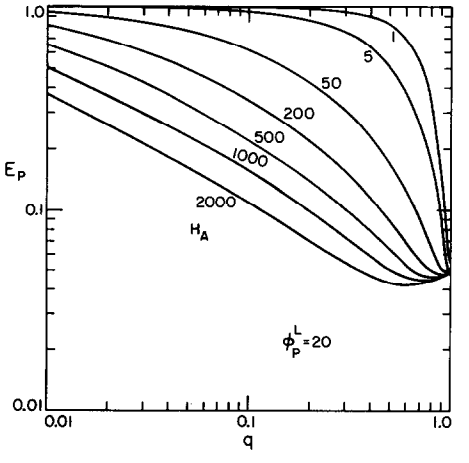

FIG. 3. The effectiveness factor for SLPC slab versus the liquid loading for $\phi_p^L = 20$ and H_A varying from 1 to 2000.

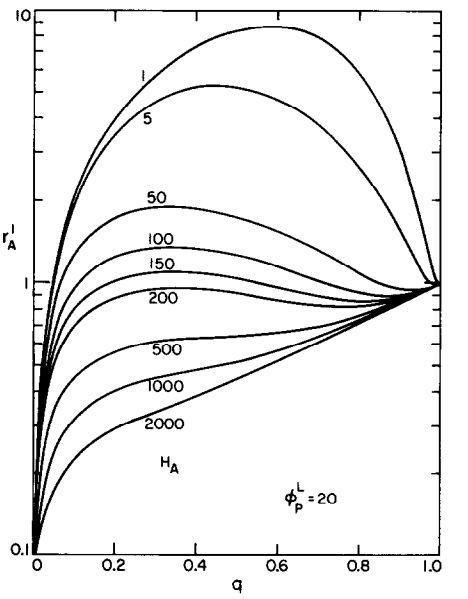

FIG. 4. The dimensionless rate of reaction in SLPC slab versus the liquid loading for $\phi_p^L = 20$ and H_A varying from 1 to 2000.

The relationship between the dimensionless rate of reaction r'_A, and the liquid loading parameter, q, for different values of the parameters H_A and ϕ_p^L is plotted in Figs. 4–6. In Fig. 4, H_A is varied from 1 to 2000 while maintaining ϕ_p^L constant at 20. Several interesting features become apparent. The dimensionless rate not only passes through a maximum as predicted by previous investigators but also goes through a minimum over a wide range of values of H_A. For low solubility of a gas, e.g., for $H_A = 1$, the minimum occurs very close to full liquid loading and the difference may not be discernable. However, as H_A increases, the maximum drops but the minimum becomes more pronounced. Thus, it may be possible to see the same rate of reaction for three different values of the liquid loading for physically realistic values of H_A. As H_A becomes very high, the curves flatten out and r'_A increases monotonically with q. It may be noted in this region of high solubility that the rate is maximum at full liquid loading thus implying that the diffusion limitations are small. It is also apparent from the figure

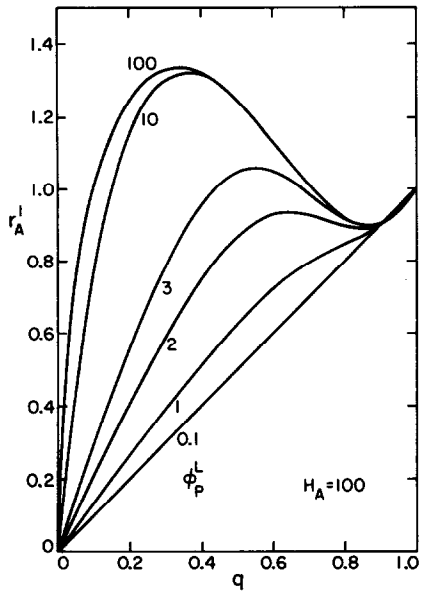

FIG. 5. The dimensionless rate of reaction in SLPC slab versus the liquid loading for $H_A = 100$ and ϕ_p^L varying from 0.1 to 100.

that the advantages of SLPC are most evident for systems of low solubility.

In Fig. 5, ϕ_p^L varies from 0.1 to 100 for a constant value of $H_A = 100$. The two limiting cases for ϕ_p^L may be obtained as follows:

(a) ϕ_p^L is small; i.e., the reaction rate is kinetic controlled. Thus E_p and $E_p^L \to 1$, and from Eq. (47)

$$r'_A = q. \tag{48}$$

The dimensionless rate thus increases linearly with q.

(b) ϕ_p^L is large, so that except for small liquid loading, ϕ_p also is large. Thus, from Eq. (47)

$$r'_A = q\frac{\phi_p^L}{\phi_p} = \left(\frac{qD_{Ae}}{C_2^0 H_A D_A^L}\right)^{1/2}. \tag{49}$$

In other words, the rate is diffusion controlled and the dimensionless rate becomes independent of the rate constant k_A.

These two limits may be seen in Fig. 5, where $\phi_p^L = 0.1$ corresponds to Eq. (48), and for $\phi_p^L > 10$, the dimensionless rate depends upon ϕ_p^L only at small q. Figure 6 is similar to Fig. 5, the only difference being that $H_A = 5$ instead of 100.

It may finally be mentioned that the richness of behavior of SLPC systems exhibited by the theoretical model developed here is not without some experimental corroboration. The existing experimental rate studies of SLPC have been compiled recently (*1*). Their Fig. 10 clearly demonstrates the variety of rate behavior observed in different SLPC systems.

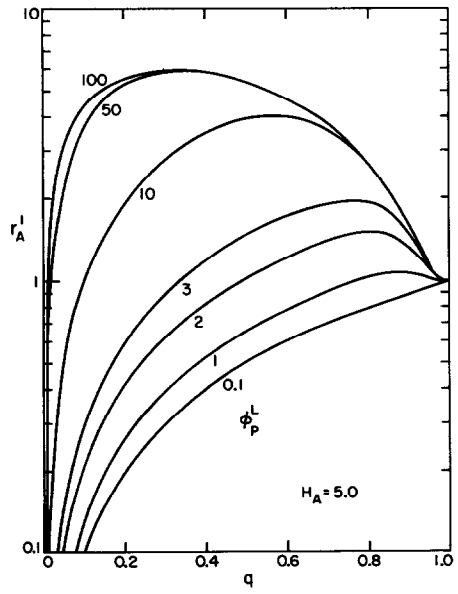

FIG. 6. The dimensionless rate of reaction in SLPC slab versus the liquid loading for $H_A = 5$ and ϕ_p^L varying from 0.1 to 100.

5. CONCLUSIONS

A theoretical model has been proposed for the transport and chemical reaction of gaseous species in supported liquid-phase catalysts. The model is valid for catalytic liquids with contract angles less than 90° supported on inert porous pellets. For gas-phase transport, the solid support along with the dispersed liquid is considered as a hypothetical porous medium. Similarly, for liquid-phase transport, the solid and the gas phases together are treated as the effective porous medium. The transport equations are based on the use of the dusty-gas model

for the gas phase and a Fickian flux model for the liquid phase. The fluxes in the two phases are assumed to be parallel. The variation of the dusty-gas constants with liquid loading is estimated using a combination of the parallel-pore model, random-pore model, and interconnected near-spherical cell description of a porous medium.

The results corroborate the existence of a maximum in the reaction rate predicted earlier and also predict other interesting features of SLPC. The predicted trends are consistent with the available experimental results.

APPENDIX: NOMENCLATURE

A	gaseous component A
a^G	mean radius of residual gas pores (m)
B	gaseous component B
$C^G_{A_s}$	concentration of A in the gas phase at the pellet surface (mol/m^3)
C^O_0	D'Arcy permeability for the dry support (m^2)
C^G_0	D'Arcy permeability for the residual gas pore space in SLPC (m^2)
C^O_1	dusty-gas Knudsen diffusion constant for the dry porous support (m)
C^G_1	dusty-gas Knudsen diffusion constant for the residual gas pore space in SLPC (m)
C^O_2	dusty-gas molecular diffusion constant for the dry porous support (dimensionless)
C^G_2	dusty-gas molecular diffusion constant for the residual gas pore space (dimensionless)
C^L_2	dusty-gas constant for liquid-phase diffusion (dimensionless)
C^G_i, C^G_A	concentration of i, A, in gas phase (mol/m^3)
C^L_i	concentration of i in the liquid phase (mol/m^3)
D^L_i, D^L_A	molecular diffusivity of i, A, in liquid phase (m^2/s)
D_{ij}, D_{AB}, D_{AI}	binary molecular diffusivity in gas phase (m^2/s)
D_{kA}	Knudsen diffusivity (Eq. (41); m^2/s)
D_{Ae}	overall effective diffusivity of A in liquid-loaded support (m^2/s)
D^G_{Ae}	effective diffusivity of A in the gas phase (m^2/s)
D^L_{Ae}	effective diffusivity of A in the liquid phase (m^2/s)
D^O_{ije}, D^O_{kie}	effective binary, Knudsen diffusivity in the dry porous support (m^2/s)
D^G_{kme}	mean effective Knudsen diffusivity (m^2/s)
D^G_{ije}, D^G_{kie}	effective binary, Knudsen diffusivity in the residual gas-pore space (m^2/s)
E_p	effectiveness factor for SLPC (dimensionless)
E^L_p	effectiveness factor for completely liquid-filled porous pellet (dimensionless)
H_i, H_A	gas–liquid partition coefficient for i, A, (mol/m^3 liquid)/mol/m^3 gas)
h	particle-shape factor = 0, 1, and 2 for planar, cylindrical, and spherical geometries, respectively
k_A	first-order homogeneous reaction rate constant (s^{-1})
L	pellet characteristic dimension (m)
M_i, M_A	molecular weight of i, A
N_A	molar flux of A in pellet (mol/m^2 s)
N^G_i, N^G_j, N^G_A	molar flux of i, j, and A, respectively, in the re-

sidual gas pore space in a liquid-loaded pellet (mol/m² s)

N_{is} molar flux of i at the pellet surface (mol/m² s)

P total pressure (Pa)

P_s pressure at the pellet surface (Pa)

q liquid-loading parameter representing the ratio of the pore volume occupied by the liquid (dimensionless)

R rate of reaction per unit volume of liquid phase (mol/m³ s)

R_g gas constant = 8.314 J/mol · K

r_A rate of reaction per unit external surface area of pellet (mol/m² s)

r_A^L rate of reaction per unit external surface area for completely liquid-filled pellet (mol/m² s)

r'_A rate of reaction defined by Eq. (47) (dimensionless)

S^O surface area of dry porous support per unit mass of a pellet (m²/kg)

S^G gas–liquid interfacial area in a liquid-loaded pellet per unit mass of dry support (m²/kg)

T temperature (K)

V^G void volume of residual gas pore space in a liquid-loaded pellet per unit mass of dry support (m³/kg)

v_i mean thermal speed of molecules of species i ($= (8R_gT/\pi M_i)^{1/2}$ m/s)

x_i, x_j, x_I mole fraction of i, j, and I, respectively, in the gas phase

x_{is} mole fraction of i in the gas phase at the pellet surface

z radial distance coordinate in a SLPC pellet (m)

Greek symbols

ϕ_p Thiele modulus for SLPC (dimensionless)

ϕ_p^L Thiele modulus for completely liquid-filled pellet (dimensionless)

θ^O porosity of dry support (m³/m³)

θ^G porosity of residual gas-pore space (m³/m³)

θ^L volume of liquid per unit pellet volume (m³/m³)

μ_m viscosity of gas mixture (Pa · s)

ν_i stoichiometric coefficient of i

ρ_p density of dry support (kg/m³)

τ tortuosity factor

τ^G tortuosity factor for residual gas pore space

τ^L tortuosity factor of the liquid phase in the pores

ACKNOWLEDGMENT

This work was supported in part by the Division of Chemical Sciences (Office of Basic Energy Sciences) of the Department of Energy under Award DE-AM03-76SF00034 P.A. No. 234.

REFERENCES

1. Villadsen, J., and Livbjerg, H., *Catal. Rev. Sci. Eng.* **17**, 203 (1978).
2. Kenney, C. N., *Chem. Reac. Eng. Rev.*, 37 (1978).
3. Livbjerg, H., Sorensen, B., and Villadsen, J., *Adv. Chem. Ser.* **133**, 242 (1974).
4. Livbjerg, H., Jensen, K. F., and Villadsen, J., *J. Catal.* **45**, 216 (1976).
5. Komiyama, H., and Inoue, H., *J. Chem. Eng. Jpn.* **8**, 310 (1975).
6. Komiyama, H., and Inoue, H., *J. Chem. Eng. Jpn. 10*, 125 (1977).
7. Parshall, G. W., "Homogeneous Catalysis: The Applications and Chemistry of Catalysis by Soluble Transition Metal Complexes." Wiley, New York, 1980.
8. Rony, P. R., *J. Catal.* **14**, 142 (1969).

9. Gerritsen, L. A., Van Meerkerk, A., Vreugdenhil, M. H., and Schollen, J. J. F., *J. Mol. Catal.* **9,** 139 (1980).
10. Acres, G. J. K., Bond, G. C., Cooper, B. J., and Dawson, J. A., *J. Catal.* **6,** 139 (1966).
11. Rony, P. R., and Roth, J. F., *J. Mol. Catal.* **1,** 13 (1975).
12. Rony, P. R., *Chem. Eng. Sci.* **23,** 1021 (1968).
13. Abed, R., and Rinker, R. G., *J. Catal.* **31,** 119 (1973).
14. Chen, O. T., and Rinker, R. G., *Chem. Eng. Sci.* **33,** 1201 (1978).
15. Mason, E. A., Malinauskas, A. P., and Evans, R. B., III, *J. Chem. Phys.* 3199 (1967).
16. Wakao, N., and Smith, J. N., *Chem. Eng. Sci.* **17,** 825 (1962).
17. Satterfield, C. N., "Mass Transfer in Heterogeneous Catalysis," MIT Press, Cambridge, Mass. 1970.
18. Jackson, R., "Transport in Porous Catalysts," Elsevier, New York, 1977.
19. Weisz, P. B., and Schwartz, A. B., *J. Catal.* **1,** 399 (1962).
20. Satterfield, C. N., Ma, Y. H., and Sherwood, T. K., *Tripartite Chem. Eng. Conf. Symp. Mass Transf. with Chem. React.*, Montreal, 26 (1968).
21. Wilson, H. D., and Rinker, R. G., *J. Catal.* **42,** 268 (1976).
22. Datta, R., and Leung, S. W.-K., *Chem. Eng. Commun.* in press.